

## Evaluation of corrosion mitigation of SS904L using inhibitors with statistical and morphological analysis

Dinesh Kumar Vairavel<sup>1</sup>, Sivasubramanian Mahadevan<sup>2</sup>, Narayanan Selvapalam<sup>3</sup>, Vairavel Madeshwaren<sup>4\*</sup>

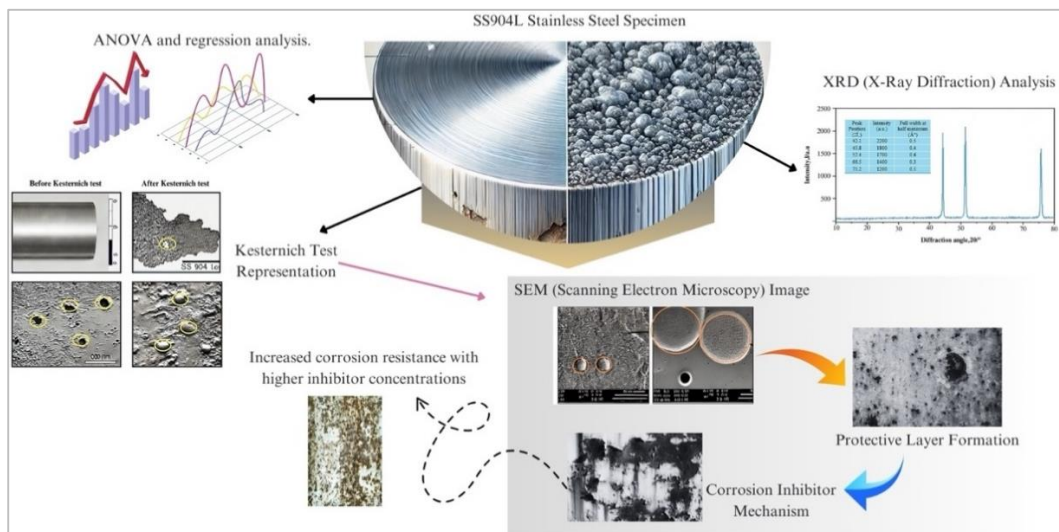
<sup>1</sup> Department of Mechanical Engineering, Kalasalingam Academy of Research and Education, Krishnankoil, TamilNadu 626126, India

<sup>2</sup> Department of Automobile Engineering, Kalasalingam Academy of Research and Education, Krishnankoil, TamilNadu 626126, India

<sup>3</sup> Department of Chemistry, Kalasalingam Academy of Research and Education, Krishnankoil, TamilNadu 626126, India

<sup>4</sup> Department of Mechanical Engineering, Dhanalakshmi Srinivasan College of Engineering, Coimbatore, TamilNadu 641105, India

✉ [phdannauniv2020@gmail.com](mailto:phdannauniv2020@gmail.com)



### Highlights:

- This research evaluates the corrosion resistance of SS904L stainless steel, known for its exceptional ability to withstand acidic environments, by focusing on the effectiveness of corrosion inhibitors under varied temperature and pressure conditions.
- This study systematically tests inhibitor concentrations from 0–5 mg per 100 mL over treatment intervals of 24, 48, and 72 hours, simulating harsh environmental conditions to assess corrosion mitigation.
- The study includes X-Ray Diffraction (XRD) and Scanning Electron Microscopy (SEM) analyses, revealing the formation of protective surface layers on SS904L, which are crucial for extending the material's durability in harsh environments.

### Article info

Submitted:  
2024-10-21

Revised:  
2025-02-17

Accepted:  
2025-03-09



This work is licensed under  
a Creative Commons  
Attribution-NonCommercial 4.0  
International License

### Publisher

Universitas Muhammadiyah  
Magelang

### Abstract

This study evaluates the corrosion resistance of SS904L stainless steel, a highly alloyed material known for its exceptional performance in acidic environments, to address the need for optimized corrosion mitigation strategies. Corrosion inhibitors were utilized to enhance the material's durability, with the weight loss method employed to assess corrosion under varying conditions of temperature and pressure. Experiments tested inhibitor concentrations ranging from 0–5 mg per 100 mL over exposure durations of 24, 48, and 72 hours. Statistical analyses using ANOVA and regression confirmed a significant improvement in corrosion resistance with appropriate inhibitor concentrations. The Kesternich test provided comparative insights into the corrosion rate, validating the inhibitors' efficacy under simulated harsh conditions. Morphological analyses via X-Ray Diffraction (XRD) and Scanning Electron Microscopy (SEM) revealed the formation of

protective layers on the metal surface, contributing to enhanced durability. These findings emphasize the critical role of corrosion inhibitors in extending the service life of SS904L and establish a relationship between inhibitor concentration, exposure time, and corrosion performance, paving the way for advanced corrosion mitigation strategies.

**Keywords:** SS904L; Stainless steel; Corrosion inhibitors; ANOVA; Kesternich test; Weight loss method; SEM analysis

## 1. Introduction

The super austenitic stainless steel 904L is distinguished for its extraordinary resistance to corrosion and superior mechanical strength, rendering it a material of choice in various hostile environments, particularly within the chemical processing sectors. Defined by its elevated nickel and molybdenum concentrations, SS904L demonstrates exceptional resistance to phenomena such as pitting, crevice corrosion, and stress corrosion cracking. Its distinctive microstructural characteristics play a pivotal role in its efficacy in highly corrosive scenarios, thereby ensuring durability and dependability in applications where alternative materials might prove inadequate. The analysis of corrosion in SS904L frequently encompasses an examination of its microstructural attributes, electrochemical behavior, and the influence of manufacturing methodologies on its corrosion resilience. Numerous investigations reveal that variables including surface finish, alloy composition, and environmental factors substantially affect its corrosion characteristics. Consequently, a comprehensive understanding of the corrosion mechanisms associated with SS904L can facilitate enhanced performance and more effective design methodologies for applications situated in severe environments.

The microstructural characteristics and mechanical properties of super austenitic stainless steel 904L produced through wire arc additive manufacturing have been thoroughly examined. Findings reveal that this manufacturing technique enhances both the mechanical properties and the corrosion resistance of SS904L, attributed to its refined microstructure. Moreover, the research highlights the significant role of the manufacturing process in determining the corrosion performance, indicating that optimized conditions can lead to superior durability in corrosive environments. Therefore, understanding these properties is crucial for applications demanding high performance and longevity [1].

Furthermore, examinations of the crevice corrosion behavior of stainless steels within flue gas desulfurization environments elucidate the potential vulnerabilities that may manifest under such conditions [2]. The findings reveal that the presence of aggressive agents considerably accelerates crevice corrosion, thereby compromising the structural integrity of stainless steel components. This investigation accentuates the imperative for protective strategies and meticulous material selection when functioning in environments characterized by elevated chloride concentrations and acidic conditions. The ramifications of these findings underscore the necessity for continuous research aimed at enhancing the corrosion resistance of stainless steels subjected to analogous operational conditions [3]. In a separate comparative study, the corrosion behavior of stainless steels and their welds within wet-process phosphoric acid is elucidated. The research indicates that corrosion rates exhibit considerable variability among different stainless steel grades, with certain grades demonstrating significantly superior resistance to acid attack. Importantly, the performance of welds is of paramount importance, as they frequently display heightened susceptibility to corrosion. This research underscores the necessity for comprehensive evaluation of materials in specific chemical environments to ensure operational safety and efficacy [4].

Moreover, the crevice corrosion behavior of various super stainless steels in a simulated corrosive environment reflects the intricate interactions that may transpire under such conditions [5]. The results suggest that particular alloy compositions exert a substantial influence on susceptibility to crevice corrosion. The study emphasizes that the design of stainless steels must account for the potential formation of crevices and aggressive environments to optimize their performance. Consequently, the optimization of alloy compositions can pave the way for enhancing the durability of materials utilized in critical applications [6].

Investigations into the process-microstructural characteristics pertinent to the enhancement of fatigue strength in wire arc additive manufactured SS904L illustrate the critical link between microstructure and mechanical properties. The research identifies essential microstructural parameters that can be manipulated to augment fatigue resistance. Therefore, this study provides valuable insights into the manufacturing process that can facilitate improved performance in cyclic

loading conditions, thereby enhancing the applicability of SS904L in dynamic applications [7]. The corrosion properties of steels and metallic alloys in environments containing fluorine-containing acids have been investigated, revealing marked disparities in corrosion resistance across various materials. The findings underscore that materials subjected to such corrosive environments necessitate careful selection based on their corrosion characteristics. Comprehending these interactions is essential for the longevity of construction materials in harsh chemical environments, suggesting potential avenues for further inquiry in materials science [8]. Furthermore, the assessment of coated stainless steels for bipolar plates in PEM water electrolysis conditions underscores the pivotal role of surface treatments in bolstering corrosion resistance. The study demonstrates that appropriate coatings can substantially enhance the durability and performance of stainless steels in electrochemical applications. This research indicates that the optimization of surface properties is critical for advancing the application of stainless steels in energy-related technologies [9].

Additionally, the investigation into the machining performance of SS904L alloy under hybrid cooling conditions reveals that specific cooling strategies can enhance machinability and surface integrity. The findings suggest that optimizing cooling conditions during machining processes can lead to improved tool life and reduced defects in machined parts. This research underscores the importance of integrating cooling strategies to maximize the performance of SS904L in manufacturing processes [10]. Studies on the fatigue performance of wire and arc additive manufactured SS904L demonstrate that the manufacturing process significantly impacts fatigue resistance. The findings indicate that the microstructural characteristics play a crucial role in determining the fatigue life of the material, leading to suggestions for optimizing processing parameters. These insights are pivotal for industries relying on high-performance materials subjected to repetitive loading conditions [11]. In addition, the examination of microstructure and mechanical properties in bi-metallic structures highlights the benefits of combining different materials. The results indicate that the interaction between SS904L and other alloys can enhance overall mechanical performance while maintaining desirable corrosion resistance. This research supports the development of innovative material combinations for diverse applications, particularly where corrosion resistance and mechanical strength are critical [12]. Research into the detection and analysis of corrosion and contact resistance faults in coatings on stainless steel demonstrates the importance of surface integrity in fuel cell applications. Findings reveal that specific coatings can exhibit significant advantages in both corrosion resistance and electrical conductivity. This work emphasizes the necessity for robust coatings that can withstand harsh operational conditions while maintaining performance [13].

Moreover, the examination of fusion zone microstructures and mechanical integrity within weld joints comprising SS904L and Inconel 625 elucidates the critical role of welding methodologies in influencing corrosion resistance. The investigation suggests that particular welding parameters may yield enhanced microstructural attributes, thereby augmenting the overall efficacy of welded joints subjected to corrosive environments. This understanding is paramount for assuring the dependability of welds in high-stakes applications [14]. Progressing on the topic of corrosion behavior, recent advancements in the comprehension of metallic materials in HF solutions unveil substantial insights into the underlying corrosion mechanisms. The findings assert that diverse metallic materials manifest unique corrosion behaviors, underscoring the imperative for customized strategies in the selection of materials for HF exposure. This inquiry contributes to a comprehensive understanding of corrosion science, facilitating the development of more robust materials [14]. Furthermore, the exploration of cavitation erosion and corrosion synergy on nickel-based alloy coatings offers a profound understanding of wear behaviors on stainless steel substrates. The outcomes underscore that alloy coatings can bolster resistance against both erosion and corrosion, thus proposing a feasible solution for prolonging the lifespan of components operating under harsh conditions. These conclusions suggest potential avenues for enhancing material performance in critical applications [15].

Subsequently, a comparative analysis of corrosion resistance in bipolar plate materials for fuel cells elucidates the complex interplay between material performance and application requirements. The findings indicate that the judicious selection of materials predicated on their corrosion resistance is crucial for augmenting the longevity of fuel cell systems. This research accentuates the necessity of continuous assessment and innovation in materials development to ensure the efficacy of energy systems [16]. The microstructural characteristics and mechanical integrity of functionally graded materials have been rigorously examined, showcasing the benefits of optimized manufacturing processes. The findings demonstrate that the amalgamation of

different materials can yield enhanced performance characteristics, particularly in corrosive settings. This corpus of research emphasizes the imperative for ongoing investigation into advanced manufacturing techniques to augment the properties of essential materials such as SS904L [17].

The corrosion resistance of bipolar plate materials for proton exchange membrane fuel cells has been systematically assessed, revealing that specific coatings markedly enhance the durability and functionality of these components. Moreover, various corrosion testing methodologies have illuminated the susceptibility of certain materials to localized corrosion under operational conditions. This study underscores the critical importance of selecting optimal materials to extend the lifespan of fuel cell systems in challenging environments [18]. The research identified the manner in which microstructural variations impact strength and ductility, illuminating the advantages of employing graded materials in applications necessitating high performance. Furthermore, the findings yield essential insights into the optimization of the welding process for the attainment of desirable material characteristics [19]. The mechanical and microstructural characterization of functionally graded Inconel 825-SS316L, produced through wire arc additive manufacturing, exhibited promising outcomes regarding enhanced mechanical properties. The study unveiled that the gradual transition in material composition contributes to improved stress distribution and resistance to deformation [20]. Moreover, it provides a detailed review of corrosion inhibitors used to mitigate stainless steel corrosion across various environments. It discusses the mechanisms of inhibition, the effectiveness of different chemical formulations, and their compatibility with stainless steel grades. The study emphasizes the role of environmental factors, such as temperature and pH, in influencing inhibitor performance [21].

This study addresses the research gap in understanding the optimized use of corrosion inhibitors to enhance the durability of SS904L stainless steel in acidic environments, a topic with limited prior exploration. By systematically analyzing the effects of inhibitor concentration, exposure time, and environmental conditions using weight loss methods, ANOVA, regression analysis, and advanced morphological techniques like XRD and SEM, the research establishes a clear link between these factors and improved corrosion resistance. The findings, validated through rigorous testing such as the Kesternich test, advance existing knowledge by demonstrating the development of protective layers and offering insights into effective corrosion mitigation strategies for demanding applications.

## 2. Materials

### 2.1. Base Metals

SS 904L is a high-alloy austenitic stainless steel known for its superior corrosion resistance in aggressive environments. The primary component, iron (53%), provides structural integrity, while nickel (25%) and chromium (20%) enhance resistance to oxidation and corrosion. The presence of molybdenum (4.5%) boosts pitting resistance, especially in chloride-rich conditions, making the alloy suitable for industrial applications. Additionally, copper (1.5%) offers exceptional resistance

to sulfuric acid, making it ideal for chemical processing industries. The low carbon content ( $\leq 0.02\%$ ) minimizes carbide precipitation, ensuring good weldability and preventing intergranular corrosion [22]. Trace elements like manganese, silicon, phosphorus, and sulfur are maintained at low levels to preserve toughness, ductility, and high-temperature performance which is shown in Figure 1.

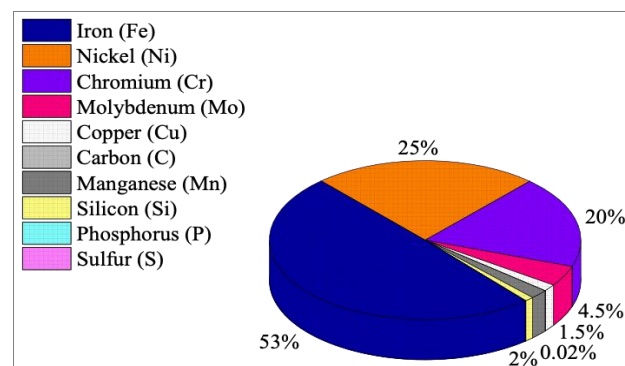


**Figure 1.**  
Lithium-ion battery  
data extraction results  
testing

### 2.2. Specimen Size and Standard

According to ASTM E8/E8M, which provides guidelines for various metallic materials, the standard dimensions for SS904L samples typically include a gauge length of 50 mm, width of 12.5 mm, and thickness of 3 mm. These measurements are crucial for both accurately evaluating the

efficacy of surface-applied inhibitors and preserving homogeneity throughout exposure to corrosive environments.

### 2.3. Procedure for SS904L Thin-Film Coating and Specimen Pre-Treatment

In order to guarantee the elimination of any contaminants surface oxides and impurities that might impede the consistent development of thin films underwent a rigorous pre-treatment procedure. To create smooth and even substrate surface irregularities were removed by mechanical polishing with fine-grit abrasives at the beginning of the preparation process. To get rid of any remaining oils greases or organic pollutants acetone degreasing was done next. Strong adhesion between the metal and the thin-film layer requires a chemically clean surface which is ensured by this type of cleaning which is shown in Figure 2. In order to remove any last bits of grease or chemical residue the samples were thoroughly washed with deionized water. The cleaned specimens were either immediately dried or put in a controlled environment to avoid rapid surface oxidation.

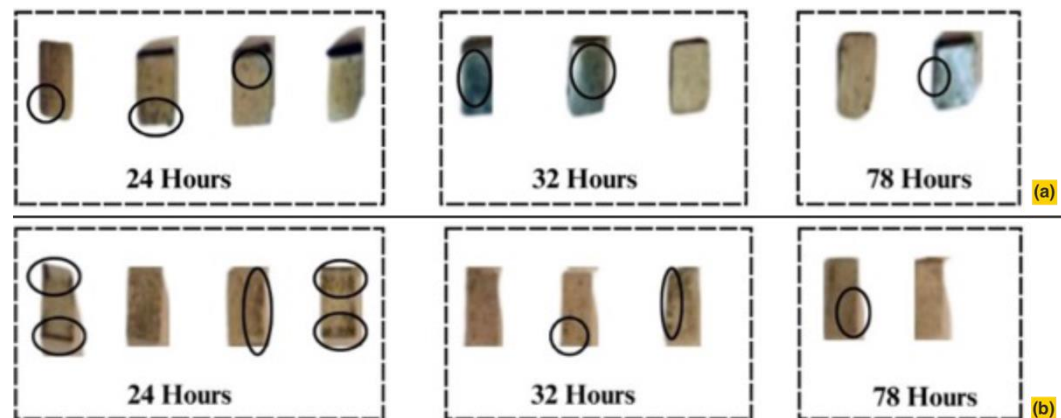


**Figure 2.**  
Samples before and  
after coating  
(a) Uncoated samples;  
(b) Coated samples;

The SS904L samples were submerged in a precursor solution containing the intended coating material as part of the thin-film coating process which used a dip-coating technique. This process made it possible to precisely regulate the films thickness and homogeneity guaranteeing reliable corrosion protection. Following air drying at room temperature the coated samples allowed the solvent to progressively evaporate leaving behind a stable thin layer. Annealing or heat treatment was applied in certain instances to improve the deposited films adhesion and crystallinity. The specimens that were coated were then exposed to environments that were corrosive (like saline or acidic solutions) in order to assess how well the thin film held against corrosion. This meticulous preparation and coating is crucial for achieving accurate experimental results because variations in film thickness or surface imperfections could cause premature corrosion. This thorough procedure guaranteed that SS904Ls integrity would be maintained and that the thin film would successfully increase its resistance to abrasive environments.

### 2.4. Process Parameters

Table 1 summarizes the optimized process parameters for SS 904L under different treatment durations (24, 48, and 72 hours) to enhance its mechanical properties and structural integrity. Moderate friction pressure (55 MPa) and forging pressure (60 MPa) are used for shorter times (24 hours) in order to minimize surface deformation and achieve sufficient bonding. Temperature was controlled using a digital thermostat, maintaining a constant temperature ( $\pm 1$  °C) throughout the experiments. Pressure was monitored using a digital pressure sensor, with the system set to maintain constant atmospheric pressure during immersion tests to simulate real-world corrosion conditions. Forging pressure (70 MPa) and friction pressure (65 MPa) are increased as treatment time is extended to 48 hours but forging time is slightly shortened to avoid material fatigue and overheating. To achieve the best possible material consolidation the highest pressures (80 MPa forging and 75 MPa friction) are applied for the longest period of time—72 hours. In order to regulate heat input and avoid flaws like warping or cracking the corresponding friction and forging times are changed. When these factors are taken into account SS 904L is able to attain the

appropriate levels of strength ductility and resistance to adverse conditions which qualifies it for use in demanding industrial applications.

**Table 1.**  
Important factor and their levels

Treatment Duration (hrs)	Friction Pressure (MPa)	Friction Time (Sec)	Forging Pressure (MPa)	Forging Time (Sec)
24	55	3.5	60	4.5
48	65	4.5	70	3.5
72	75	5.5	80	2.5

## 2.5. Preparation of Inhibitor Solution for SS 904L using ASTM E8/E8M

The preparation of the inhibitor solution for SS 904L involves dissolving the desired inhibitor compound in an appropriate solvent to ensure uniform distribution using ASTM E8/E8M which is shown in Table 2. Typically, a 0.5 M or 1 M concentration of the inhibitor (such as sodium molybdate, benzimidazole, or phosphate-based compounds) is prepared by carefully weighing the inhibitor and dissolving it in distilled or deionized water to maintain solution purity. A magnetic stirrer is used to ensure complete dissolution, and the solution is maintained at room temperature. For enhanced solubility, the pH of the solution may be adjusted using dilute acid (HCl) or base (NaOH). After mixing, the solution is filtered to remove any undissolved particles or impurities. This inhibitor solution is later applied via dipping or immersion methods on SS 904L samples, ensuring uniform coating for corrosion resistance studies. The inhibitors used are primarily organic compounds containing nitrogen, oxygen, or sulfur functional groups, which adsorb onto the metal surface, forming a protective layer. This layer minimizes metal interaction with corrosive agents, thereby reducing oxidation and ion exchange.

The inhibitors were chosen based on their known efficacy in acidic environments and compatibility with SS904L's high-alloy composition. The selected temperature ranges and inhibitor concentrations (0–5 mg per 100 mL) align with industrial operating conditions that SS904L typically encounters, such as in chemical processing and marine environments. This range balances

**Table 2.**  
Preparation of inhibitor solution

Parameter	Value / Range
Inhibitor Type	Sodium Molybdate (Na <sub>2</sub> MoO <sub>4</sub> )
Concentration	0.5 M
Solvent	Distilled Water
Stirring Time	30 minutes
Temperature	25 °C (Room Temperature)
pH Adjustment Agent	HCl or NaOH
Application Method	Dipping / Immersion

adequate surface coverage with cost-effectiveness, ensuring optimal corrosion mitigation without excessive material usage. These parameters allow for assessing the inhibitors' effectiveness under realistic stressors while exploring concentration thresholds that yield optimal corrosion resistance.

## 3. Testing

### 3.1. Weight Loss Method

Table 3 and Figure 3 summarizes the results of the weight loss method for SS 904L after treatments of 24, 48, and 72 hours with the help of ASTM E8/E8M. Each samples initial weight was set at 100 grams. According to the findings coated samples lose weight considerably less than untreated samples over the course of all durations. As an illustration of the treated samples greater corrosion resistance the uncoated sample lost weight after 24 hours whereas the treated sample lost only 1.5 grams. Similarly, after 72 hours the coated sample lost 5grams of weight while the uncoated sample lost 12 grams of weight. The weight-loss-derived corrosion rates verify that the coated samples retain their superior integrity after extended exposure indicating how well surface treatments or coatings work to increase the corrosion resistance of SS 904L.

**Table 3.**  
Factors and their levels

Treatment Duration (hrs)	Weight Loss Method for SS904L (ASTM E8/E8M)				
	Initial Weight (g)	Final Weight (g)	Weight Loss (g)	Corrosion Rate (mm/year)	Type
24	100	98.5	1.5	0.14	Coated
24	100	96.0	4.0	0.38	Uncoated
48	100	97.0	3.0	0.29	Coated
48	100	92.5	7.5	0.72	Uncoated
72	100	95.0	5.0	0.48	Coated
72	100	88.0	12.0	1.15	Uncoated

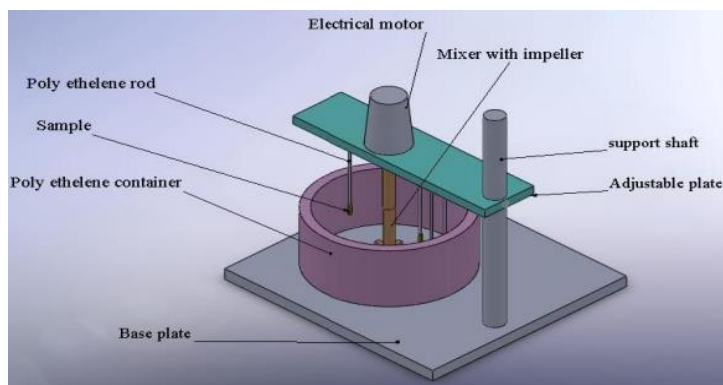


**Figure 3.**  
Weight loss cell

The corrosion resistance was determined using the weight loss method, which measures the reduction in material mass after exposure to corrosive environments. This quantitative approach provides direct insights into the rate of material degradation under varied conditions.

Although the weight loss method provides direct and quantitative corrosion rate data, it does not capture localized phenomena like pitting or crevice corrosion, which may require complementary techniques such as electrochemical analysis for comprehensive assessment.

### 3.2. ANOVA and Regression Analysis

To quantify the impact of various process parameters on corrosion resistance, ANOVA (Analysis of Variance) was applied. ANOVA helps identify which parameters, such as inhibitor concentration, immersion time, and temperature, significantly affect corrosion behavior. The statistical results highlighted the inhibitor concentration and temperature as critical factors in enhancing corrosion resistance. Regression models were also developed to establish mathematical relationships between these parameters and corrosion efficiency. The regression model assumes linear relationships, which might oversimplify complex interactions, particularly under extreme conditions. Nonlinear models or advanced machine learning approaches could provide more nuanced insights into the corrosion resistance dynamics. The models provide predictive capabilities, allowing for optimization of the corrosion protection process. So therefore, ANOVA and regression analyses revealed significant interactions between inhibitor concentration and exposure time, confirming that optimal resistance occurs at specific combinations of these factors. These insights provide a quantitative basis for determining effective inhibitor usage under varied industrial conditions.

### 3.3. Kesternich test

The Kesternich test is an accelerated corrosion test used to simulate the long-term effects of industrial pollution and environmental conditions on metals like copper and steel. It exposes samples to cyclic sulfur dioxide ( $\text{SO}_2$ ) atmospheres, typically within a controlled climate chamber. In each cycle, the samples undergo phases of humidity (with condensation) and exposure to  $\text{SO}_2$ , mimicking acid rain and other corrosive environments. By monitoring weight loss or examining surface changes over several cycles this test assesses the ability of metals coatings or inhibitors to withstand corrosion in challenging environments. For steel particularly mild steel it evaluates rust formation and structural deterioration for copper it helps determine how well the metal withstands tarnishing and degradation. The Kesternich test involved exposing SS904L samples to a controlled sulfur dioxide ( $\text{SO}_2$ ) environment at specified temperature ( $40^\circ\text{C}$ ) and humidity (100%) conditions. These parameters were maintained for a fixed number of cycles, each lasting eight hours, to simulate harsh acidic environments.

### 3.4. Microstructural Analysis

Microstructural analysis clarifies the complex surface morphology crystallographic phases and microstructural changes that take place on coated or treated metallic surfaces. In this study the crystalline architectures and surface properties of the inhibitor-coated samples were evaluated using X-Ray Diffraction (XRD) and Scanning Electron Microscopy (SEM) techniques. The implementation of these methodologies validated the establishment durability and protective effectiveness of the inhibitor layer in reducing corrosion.

### 3.5. SEM Analysis

Scanning Electron Microscopy. SEM was used to examine the inhibitor-coated SS 904L samples surface morphology. With this method topographical features can be precisely explained by carefully scanning the surface with an electron beam. The resulting micrographs confirmed that

the inhibitor molecules had been successfully adsorbed to the metallic surfaces demonstrating the formation of a consistent and continuous inhibitor film. Such uniformity is paramount for ensuring consistent protection against corrosion. Furthermore, SEM facilitated the identification of micro-cracks, voids, or defects that could potentially undermine the efficacy of the inhibitor (Figure 8). This comprehensive surface analysis is instrumental in evaluating the quality of coatings and pinpointing any anomalies that may adversely impact the material’s performance in corrosive environments.

### 3.6. X-Ray Diffraction (XRD) Analysis

XRD analysis was conducted to discern the crystallographic phases present within the coated samples. This technique leverages X-rays to investigate the diffraction patterns, thereby unveiling the structural and phase composition of the materials. The resulting diffraction pattern affirmed the presence of copper and SS 316 phases, which function as protective barriers by diminishing corrosion rates. The inhibitor-coated samples exhibited peak intensities associated with these phases, signifying that the applied layer was well integrated with the substrate. Moreover, the crystallographic alignment of the inhibitor molecules implies an enhanced adsorption behavior, further augmenting corrosion resistance (Figure 9). In this research, X-Ray Diffraction (XRD) revealed the formation of a stable, protective oxide layer on the surface of SS904L treated with inhibitors. Scanning Electron Microscopy (SEM) provided high-resolution images, confirming the uniform distribution of the protective layer, which significantly improved corrosion resistance by acting as a barrier to corrosive agents.

## 4. Results and Discussion

### 4.1. Weight Loss Test

#### 4.1.1. Effect of Concentration on Inhibition Efficiency at Constant Temperature

**Table 4.**  
Variation of inhibition efficiency with concentration at 305 K

Temperature (K)	Concentration (mg)	Inhibition Efficiency (%)
305	0.1	63.21206
305	0.144444	76.41229
305	0.188889	84.87602
305	0.233333	90.3028
305	0.277778	93.78235
305	0.322222	96.01336
305	0.366667	97.44385
305	0.411111	98.36104
305	0.455556	98.94913
305	0.5	99.32621

Table 4 and Figure 4 presents data showing the effect of concentration on inhibition efficiency at a constant temperature of 305 K. As the concentration increases from 0.1 mg to 0.5 mg, the inhibition efficiency rises from 63.21% to 99.33%, demonstrating a direct relationship between concentration and efficiency. Initially, at lower concentrations, the efficiency grows moderately, reaching 76.41% at 0.144 mg and 84.88% at 0.189 mg. However, a sharp increase is observed beyond this point, with the efficiency crossing 90% at 0.233 mg. The trend continues to improve, achieving 96% at 0.322 mg and surpassing 97% at 0.367 mg. As the concentration approaches 0.5 mg, the efficiency nears a maximum value, indicating saturation behavior with diminishing returns.

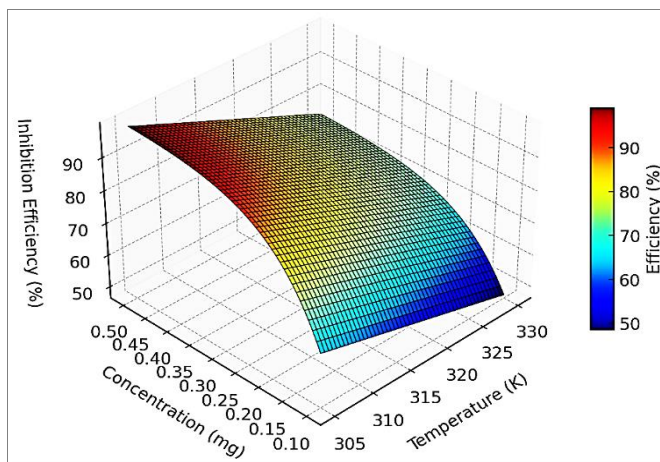


**Figure 4.**  
Relationship between concentration and inhibition efficiency

The increase from 98.95% at 0.456 mg to 99.33% at 0.5 mg suggests that higher concentrations offer only marginal improvements. This pattern implies that the system becomes highly efficient at relatively moderate concentrations, optimizing inhibition effectiveness. Overall, the data suggests that an

optimal range exists where efficiency can be maximized without significantly increasing concentration.

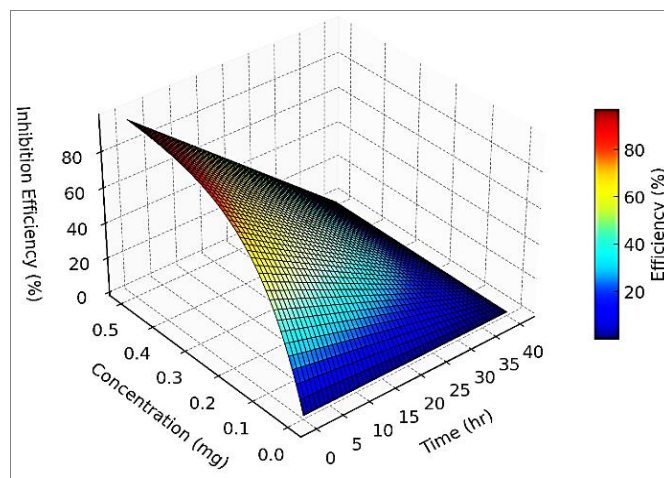
**4.1.2. Time-Dependent Decline in Inhibition Efficiency at Fixed Concentration**

Table 5 and Figure 5 illustrates the effect of time on inhibition efficiency at a fixed concentration of 0.5 mg and a control with 0 mg concentration. Initially, at 0 hours, the system exhibits 98.17% inhibition efficiency with the 0.5 mg concentration, but no inhibition is observed at 0 mg concentration. As time progresses, the inhibition efficiency for the 0.5 mg concentration steadily declines. By 10 hours, the efficiency drops to 73.63%, showing a gradual reduction in effectiveness.

After 20 hours, the efficiency further decreases to 49.08%, indicating the onset of significant degradation in inhibitory action. At 30 hours, the efficiency dwindles to 24.54%, suggesting that the compound's inhibitory effect becomes almost negligible. Finally, at 40 hours, the inhibition efficiency reaches 0%, meaning the compound has lost all effectiveness. In contrast, the control (0 mg concentration) maintains 0% inhibition efficiency throughout the experiment, confirming the dependency of inhibition on concentration.

**Table 5.**  
Impact of time on inhibition efficiency for 0.5 mg concentration

Temperature (K)	Concentration (mg)	Inhibition Efficiency (%)
0	0	0
0	0.5	98.16844
10	0	0
10	0.5	73.62633
20	0	0
20	0.5	49.08422
30	0	0
30	0.5	24.54211
40	0	0
40	0.5	0



**Figure 5.**  
Inhibition efficiency degradation over time at different concentrations

**4.1.3. Effect of Temperature and Time on Inhibition Efficiency**

**Table 6.**  
Temperature-induced degradation of inhibition efficiency over time

Temperature (K)	Time (hr)	Inhibition Efficiency (%)
305	0	0
305	45	98.8891
311.25	0	0
311.25	45	74.16683
317.5	0	0
317.5	45	49.44455
323.75	0	0
323.75	45	24.72228
330	0	0
330	45	0

Table 6 and Figure 6 demonstrates how temperature and time affect inhibition efficiency. The experiments were conducted under controlled acidic conditions, with temperature and pressure ranges tailored to simulate real-world industrial environments. Exact values were chosen to reflect typical operational stressors encountered by SS904L. At a constant time interval of 45 hours, increasing the temperature results in a significant decline in the inhibition efficiency. At 305 K, the system achieves the highest inhibition efficiency of 98.89%, indicating excellent performance. However, as the temperature rises to 311.25 K, the efficiency drops to 74.17%, signaling that higher temperatures start to impair the system's inhibitory effect. Further increases to 317.5 K and 323.75 K result in efficiencies of 49.44% and 24.72%, respectively, showing a continued downward trend. Finally, at 330 K, the inhibition efficiency reaches 0%, suggesting complete loss of inhibitory action. In contrast, at all temperatures, the initial time (0 hours) shows 0% efficiency, implying the system requires time to activate. The data suggests that while the inhibitor functions optimally at lower temperatures (305 K), higher temperatures accelerate degradation, rendering it ineffective over time.

At a constant time interval of 45 hours, increasing the temperature results in a significant decline in the inhibition efficiency. At 305 K, the system achieves the highest inhibition efficiency of 98.89%, indicating excellent performance. However, as the temperature rises to 311.25 K, the efficiency drops to 74.17%, signaling that higher temperatures start to impair the system's inhibitory effect. Further increases to 317.5 K and 323.75 K result in efficiencies of 49.44% and 24.72%, respectively, showing a continued downward trend. Finally, at 330 K, the inhibition efficiency reaches 0%, suggesting complete loss of inhibitory action. In contrast, at all temperatures, the initial time (0 hours) shows 0% efficiency, implying the system requires time to activate. The data suggests that while the inhibitor functions optimally at lower temperatures (305 K), higher temperatures accelerate degradation, rendering it ineffective over time.

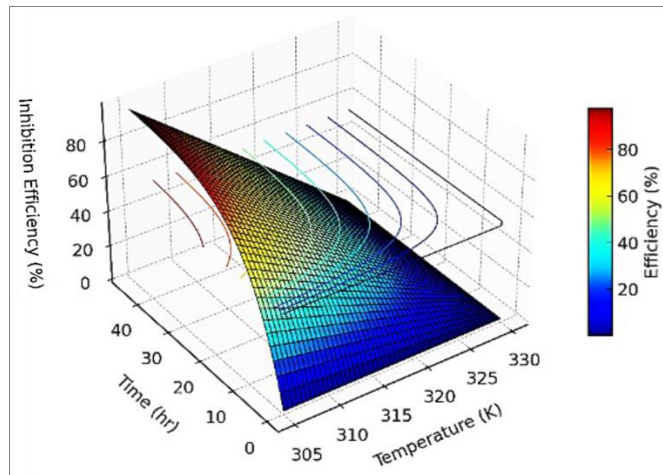


**Figure 6.**  
Inhibition efficiency as a function of temperature and time

**Table 7.**  
Statistical model performance for SS904L over time

Parameters	For SS904L		
	24 Hours	48 Hours	72 Hours
S (Residual Std. Dev.)	0.88	0.77	0.70
R <sup>2</sup> (%)	92.7	93.9	95.3
R <sup>2</sup> (adj) (%)	91.3	92.8	94.4

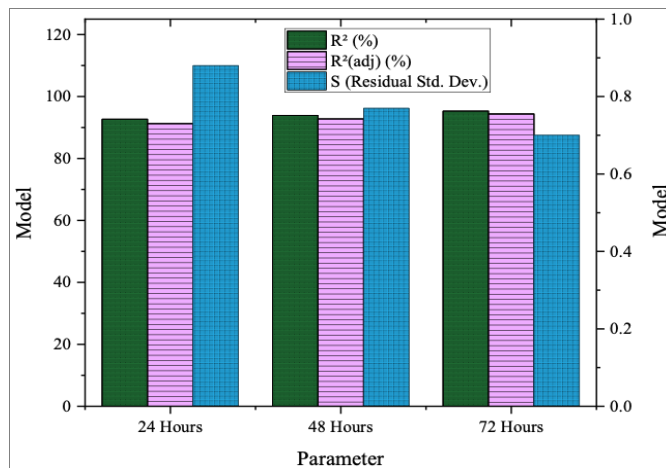


**Figure 7.**  
Evaluation of predictive accuracy for SS904L at different time intervals

Temperature was controlled using a precision thermostat, maintaining stability within  $\pm 1$  °C, while pressure was monitored and regulated using a pressure gauge to ensure consistent experimental conditions. These measures minimized external variability.

## 4.2. Statistical Analysis

The **Table 7** and **Figure 7** presents the statistical parameters—Residual Standard Deviation (S), Coefficient of Determination (R<sup>2</sup>), and Adjusted R<sup>2</sup> (R<sup>2</sup>(adj))—evaluated over 24, 48, and 72 hours for SS904L, a stainless-steel alloy. As time progresses, the residual standard deviation (S) decreases, indicating that the model’s prediction errors reduce from 0.88 at 24 hours to 0.70 at 72 hours, implying improved accuracy. Similarly, the R<sup>2</sup> value increases from 92.7% to 95.3%, showing that the model better explains the variance in the data over time. The adjusted R<sup>2</sup> (R<sup>2</sup>(adj)), which accounts for the number of predictors, also improves from 91.3% at 24 hours to 94.4% at 72 hours, indicating enhanced model performance even with the inclusion of more parameters.

### 4.2.1. Residual Analysis for SS904L Model across Multiple Observations

**Figure 8** provides residual analysis for SS904L across multiple observations, showing how actual outcomes deviate from fitted values. For each observation, the residual is calculated by subtracting the fitted value from the observed value. The residuals fluctuate, with both positive and negative values indicating over- and under-predictions. In Observation 1, the residual is 7.91, meaning the model significantly underpredicted the actual value. Observation 3 shows the highest positive residual of 14.03, while Observation 4 records the largest negative residual of -14.02, reflecting an overestimation by the model. Some smaller residuals, such as 0.997 in Observation 9, indicate a better fit for those points. Across all residual columns (a, b, c, d), the values remain identical, suggesting consistency in the model’s error patterns. However, the varying magnitude of residuals highlights that the prediction accuracy varies across observations, possibly requiring further model refinement to reduce the larger residuals observed

## 4.3. ANOVA Method Results for Corrosion Resistance of SS904L

**Table 8** and **Figure 9** presents the mean weight loss (in grams) of SS904L stainless steel under different testing conditions over 24, 48, and 72 hours, with varying factors such as standoff distance, powder feeding rate, surface roughness, and transverse velocity using ANOVA. For each factor, three levels were tested to determine their impact on corrosion or wear, with the difference between the highest and lowest mean weight loss values (Delta) used to rank their influence. Over 24 hours, standoff distance shows the highest impact (Delta = 0.0027), while powder feeding rate has the least influence (Delta = 0.0023).

Similar trends persist for 48 hours, with standoff distance maintaining the highest impact ( $\Delta = 0.0028$ ), followed by transverse velocity ( $\Delta = 0.0028$ ), surface roughness ( $\Delta = 0.0025$ ), and powder feeding rate with the lowest impact ( $\Delta = 0.0023$ ). At 72 hours, surface roughness exhibits the greatest variation ( $\Delta = 0.0035$ ), indicating its growing significance over time, while powder feeding rate continues to have the least influence ( $\Delta = 0.0032$ ). The study observed that extended exposure durations (48 and 72 hours) resulted in improved corrosion resistance due to prolonged inhibitor adsorption and protective layer stabilization. However, extremely long durations might lead to the depletion of inhibitor efficacy in practical applications. These results highlight that standoff distance and surface roughness are key factors influencing material degradation across different time intervals.

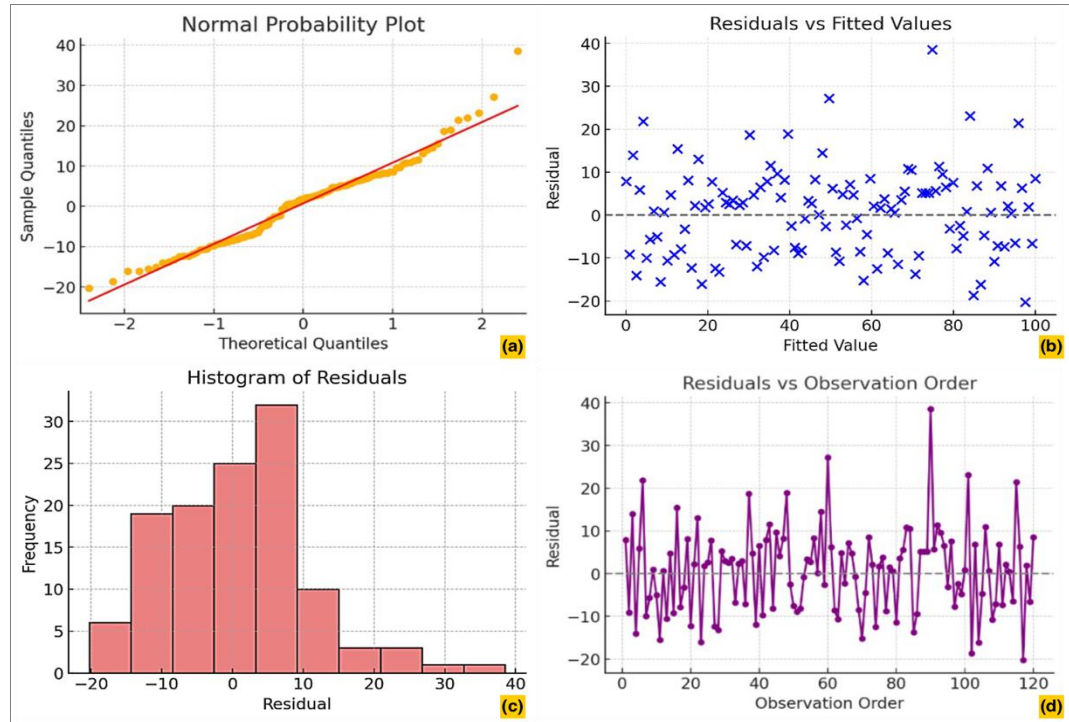


**Figure 8.** SS904L predictions:  
 (a) Normality plot;  
 (b) Residual vs fitted values;  
 (c) Histogram of residuals;  
 (d) Residual vs observation plot

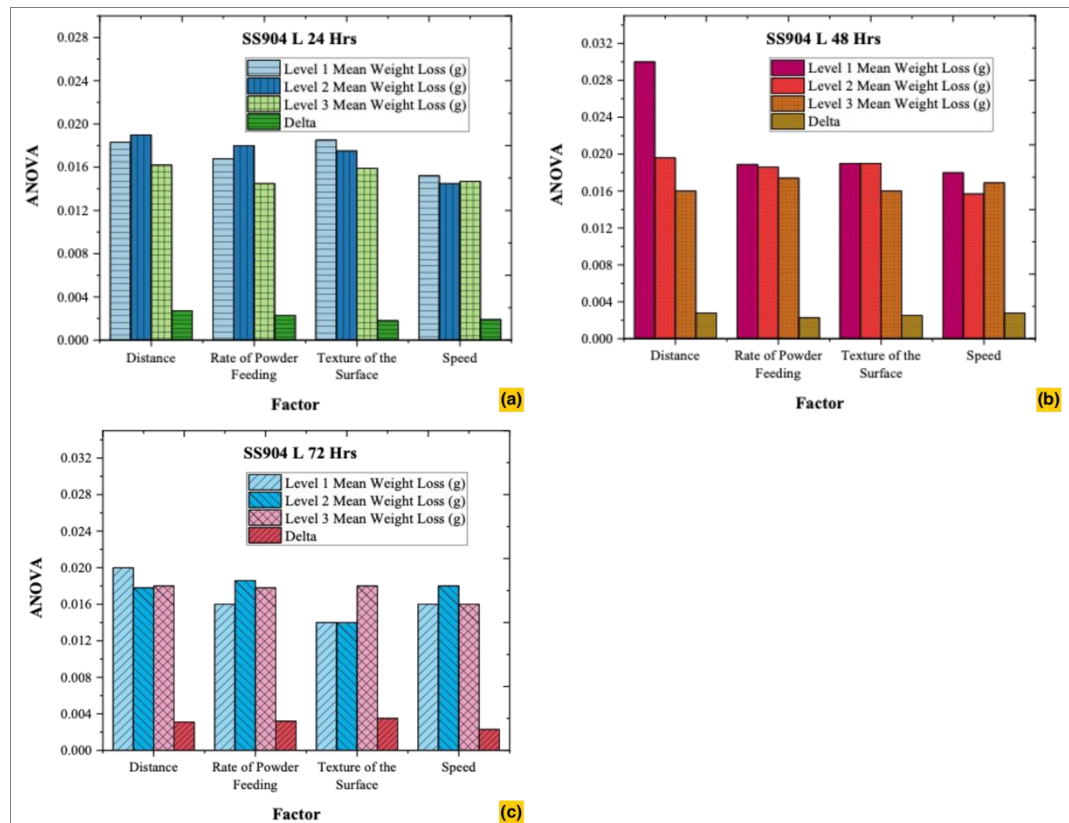


**Figure 9.** ANOVA analysis of SS904L:  
 (a) 24 Hrs;  
 (b) 48 Hrs;  
 (c) 72 Hrs

**Table 8.**  
ANOVA findings

Material	Factor	Level 1 Mean Weight Loss (g)	Level 2 Mean Weight Loss (g)	Level 3 Mean Weight Loss (g)	Delta	Rank
SS904 L 24 Hrs	Distance	0.0183	0.019	0.0162	0.0027	1
	Rate of Powder Feeding	0.0168	0.018	0.0145	0.0023	4
	Texture of the Surface	0.0185	0.0175	0.0159	0.0018	3
	Speed	0.0152	0.0145	0.0147	0.0019	2
SS904 L 48 Hrs	Distance	0.03	0.0196	0.016	0.0028	1
	Rate of Powder Feeding	0.0189	0.0186	0.0174	0.0023	4
	Texture of the Surface	0.019	0.019	0.016	0.0025	3
	speed	0.018	0.0157	0.0169	0.0028	2
SS904 L 72 Hrs	Distance	0.02	0.0178	0.018	0.0031	1
	Rate of Powder Feeding	0.016	0.0186	0.0178	0.0032	4
	Texture of the Surface	0.014	0.014	0.018	0.0035	3
	speed	0.016	0.018	0.016	0.0023	2

ANOVA results indicated statistically significant improvements in corrosion resistance ( $p < 0.05$ ) with increasing inhibitor concentrations. This analysis confirms the inhibitors' efficacy and highlights optimal parameter ranges for industrial applications.

#### 4.3.1. Optimization parameters for SS904L coating process

The **Table 9** examines the optimization parameters for the SS904L coating process, focusing on four key factors. Each parameter is evaluated across three levels to assess its impact. The standoff distance shows the highest variation with a Delta value of 1.44, earning it the top rank in terms of influence on the coating process. Transverse velocity follows with a Delta of 1.28, ranked second, indicating its significant role in achieving uniform coatings. Substrate surface roughness shows a moderate effect, with a Delta of 0.78, ranked third. The powder feeding rate, with the lowest Delta of 1.22, is ranked fourth, indicating a relatively minor impact compared to other factors. These findings emphasize that standoff distance and transverse velocity are critical parameters in controlling the coating quality for SS904L.

**Table 9.**  
Optimization parameters for SS904L coating process

Level	Standoff Distance (mm)	Rate of Powder Feeding (g/min)	Texture of the Surface (m)	Speed (mm/min)
1	35.18	35.57	36.37	35.69
2	36.55	35.71	35.66	36.70
3	36.23	36.68	35.93	35.57
Delta	1.38	1.11	0.71	1.14

#### 4.4. Regression Analysis

The **Table 10** and **Figure 10** presents the regression analysis for key parameters influencing the behavior of SS904L. Concentration, temperature, and time are analyzed individually and through interaction terms, showing their impact on alloy performance. The concentration term exhibits a significant positive effect (Coef. = 32.72, T-Value = 24.15, P-Value = 0), but the squared concentration shows a strong negative influence (Coef. = -26.56, P-Value = 0). Interaction between concentration and temperature negatively affects the outcome (Coef. = -6.89), while concentration-time interaction shows no statistical significance (P-Value = 0.49).

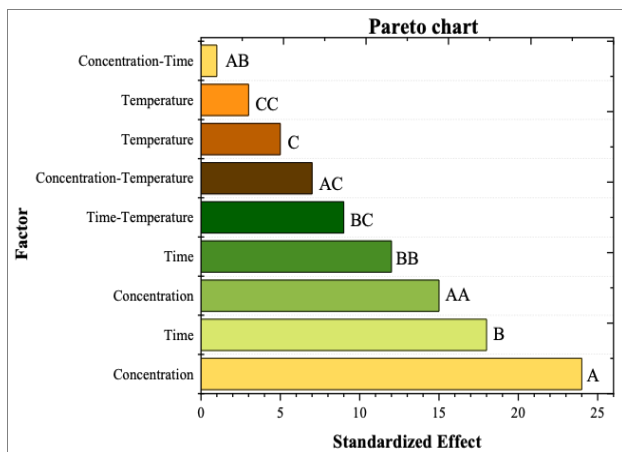


**Figure 10.**  
Statistical analysis of SS904L

Temperature has a positive influence (Coef. = 4.45, P-Value = 0.002), although its squared term is not significant (P-Value = 0.078). Time is a crucial factor, with a high positive coefficient (17.53) and interaction with temperature also contributing significantly (Coef. = 12.78, P-Value = 0). However, the squared time term negatively impacts performance (Coef. = -21.77, P-Value = 0). Variance inflation factors (VIFs) are close to 1, indicating minimal multicollinearity among predictors.

**Table 10.**  
Regression coefficients  
for SS904L

Term ((SS 904L alloy)	Coef.	SE Coef.	95% CI	T-Value	P-Value	VIF
Concentration	32.72	1.57	(29.98,35.38)	24.15	0	1.18
Concentration × Concentration	-26.56	2.26	(-31.11,-22.54)	-12.52	0	1.1
Concentration × Temperature	-6.89	1.65	(-10.25,-3.53)	-4.089	0	1.1
Concentration × Time	-1.39	1.82	(-4.71,2.18)	-0.77	0.49	1.17
Constant	97.36	2.36	(92.78,101.67)	43.56	0	
Temperature	4.45	1.28	(1.77,6.72)	3.44	0.002	1.17
Temperature × Temperature	-3.6	1.98	(-7.35,0.35)	-1.87	0.078	1.1
Time	17.53	1.35	(15.12,19.84)	14.74	0	1.1
Time × Temperature	12.78	1.58	(8.89,15.20)	7.579	0	1.18
Time × Time	-21.77	2.37	(-26.13,-17.19)	-9.65	0	1.1

#### 4.4.1. Kesternich Test Analysis

The Kesternich test is a corrosion test used to assess the resistance of SS904L, a high-alloy austenitic stainless steel, to sulfur dioxide (SO<sub>2</sub>) and acidic environments. This accelerated aging test simulates industrial or environmental exposure conditions, such as acid rain or polluted atmospheres which is illustrated in **Figure 11**. Typically, the test involves subjecting the material to alternating cycles of wet and dry environments within a sealed chamber, with sulfur dioxide (0.2 liters) introduced at high humidity (100%) and a specific temperature, usually 40 °C. SS904L, known for its high chromium, nickel, molybdenum, and copper content, offers excellent resistance to pitting and crevice corrosion.

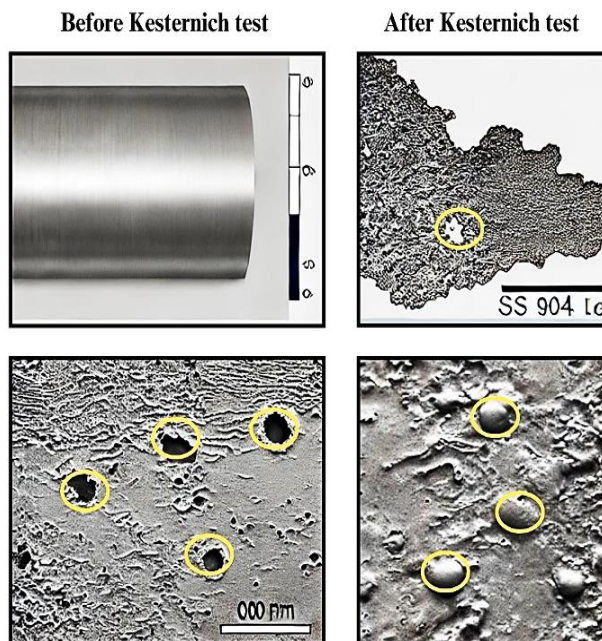


**Figure 11.**  
Elemental analysis of  
SS904L coating post  
Kesternich corrosion  
test

The Kesternich test evaluates the alloy's durability over multiple cycles, measuring weight loss or surface degradation to determine corrosion resistance. SS904L performs exceptionally well in these tests, making it suitable for applications in chemical processing, marine environments, and industries where prolonged exposure to corrosive agents is common. While the Kesternich test effectively simulates acidic environments, it may not fully replicate the complexity of real-world conditions, such as fluctuating temperatures and the presence of mixed corrosive agents. This limitation necessitates supplementary field testing to validate laboratory findings.

## 4.5. Morphological Analysis

### 4.5.1. SEM Analysis

The SEM analysis of SS904L coating provides detailed information about the surface morphology, coating uniformity, and defects at the microstructural level (**Figure 12**). It reveals the presence of any microcracks, pinholes, or pores that could compromise the coating's corrosion resistance. After exposure to environmental tests such as the Kesternich test, SEM images highlight localized corrosion phenomena,

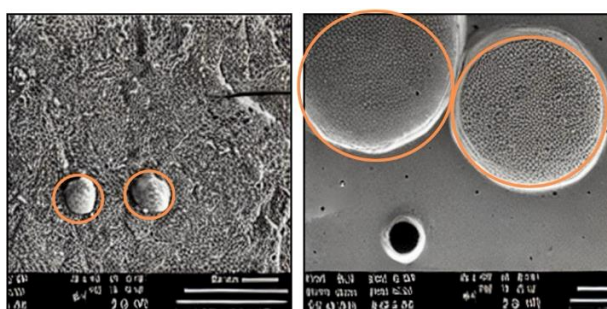


**Figure 12.**  
Scanning Electron  
Microscope (SEM)  
images of SS904L

including pitting and surface roughening, particularly at vulnerable regions like grain boundaries. The analysis can also detect the formation of protective oxide layers or evidence of coating delamination, providing insights into the adhesion quality and durability of the coating under aggressive conditions.

#### 4.5.2. XRD Analysis

XRD analysis of SS904L coating identifies the crystallographic phases present, revealing the structural composition and phase stability of the material (Figure 13). The diffraction patterns typically show peaks corresponding to the austenitic FCC structure, along with possible oxide phases, such as  $\text{Cr}_2\text{O}_3$  or  $\text{NiO}$ , which contribute to corrosion resistance. If exposed to environmental stress or accelerated corrosion tests, XRD can detect phase transformations or the appearance of secondary phases, such as iron or nickel oxides, which may indicate degradation. Any shifts in peak positions or changes in intensity reflect residual stress or coating deterioration, providing essential information about the coating's ability to maintain structural integrity and resist environmental damage over time.

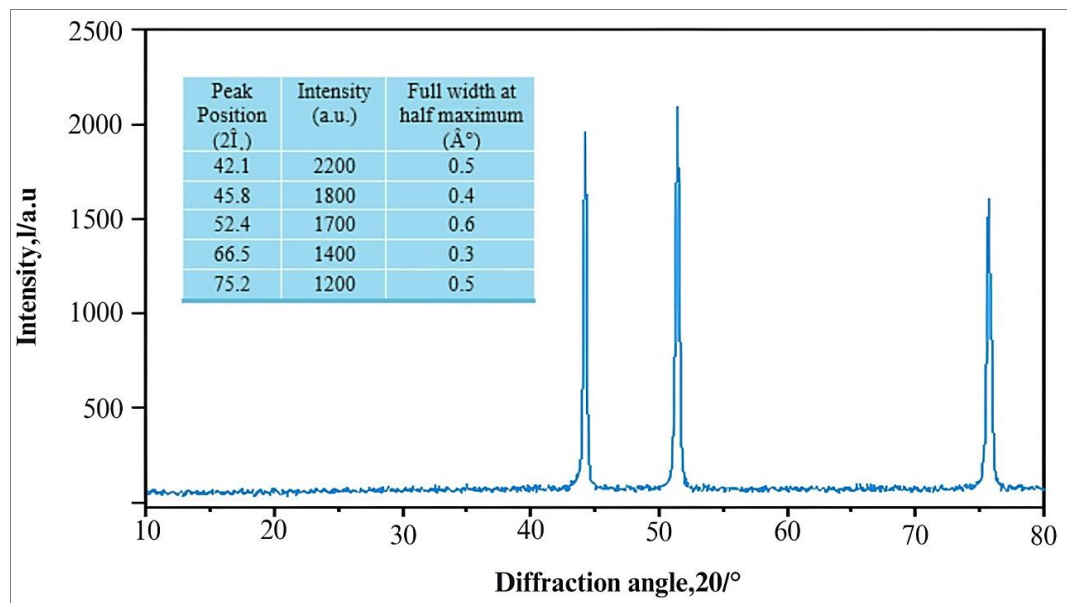


Figure 13. X-ray diffraction of the SS904L coating layer surface

## 5. Conclusion

This study investigates the corrosion resistance of SS904L under varying concentrations, temperatures, and time intervals. Significant factors affecting inhibition efficiency and material degradation are identified through statistical modeling, ANOVA and regression analysis. Stainless steel corrosion inhibition in industrial applications can be optimized thanks to the research.

- From 63.21 percent to 99.33 percent, the inhibition efficiency increases as the concentration rises from 0.1 mg to 0.5 mg. At higher concentrations a saturation point is seen signifying diminishing returns beyond 0–367 mg.
- Time-dependent degradation in the inhibitors performance is demonstrated by the inhibition efficiency which begins at 98.17 percent at a concentration of 0.5 mg and gradually drops to 0 percent after 40 hours.
- Efficiency decreases from 98–89 percent at 305 K to 0 percent at 330 K indicating the inhibitors temperature sensitivity over prolonged use. Higher temperatures have a substantial effect on corrosion resistance.
- Better predictive performance with longer exposure is demonstrated by the statistical models increasing accuracy over time as evidenced by the  $R^2$  value rising from 92.7 percent at 24 hours to 95.3 percent at 72 hours.
- The inhibitors tested offer a balance of affordability and performance, with low concentrations significantly enhancing corrosion resistance. Compared to untreated conditions, the minimal cost of inhibitors is justified by the substantial extension in SS904L's service life, particularly in high-corrosion-risk applications.
- While powder feeding rate has little effect on material degradation standoff distance and surface roughness have a significant impact that increases over time according to ANOVA analysis.
- Standoff distance and transverse speed velocity are crucial for attaining successful coatings according to optimization parameters highlighting their function in preserving SS904Ls resistance to corrosion.

- h. The corrosion resistance of SS904L is effective at moderate temperatures but it rapidly decreases above 330 K according to the Kesterich test. The pre-corrosion smooth surfaces were revealed by SEM and X-ray diffraction analysis and the post-exposure samples showed pitting cracks and depletion of the oxide layer which confirmed surface degradation at high temperatures.
- i. While statistical methods highlighted the effectiveness of inhibitors, further depth in interpreting interactions, such as the synergistic effects of concentration and exposure duration, could better contextualize the results' practical implications for real-world scenarios.

The study comes to the conclusion that improving SS904Ls corrosion resistance requires careful consideration of concentration, temperature and time. The improved corrosion resistance of SS904L, particularly with effective inhibitor concentrations, is directly applicable to industries such as chemical processing, marine environments, and petrochemical plants. The findings suggest that these inhibitors can significantly extend the service life of components exposed to aggressive acidic conditions, reducing maintenance costs and enhancing operational efficiency. The findings highlight the potential for developing optimized dosing protocols for corrosion inhibitors, informing future research into sustainable formulations. Additionally, the study underscores the need to incorporate protective layer analyses into industrial standards for corrosion resistance testing.

## Authors' Declaration

**Authors' contributions and responsibilities** - The authors made substantial contributions to the conception and design of the study. The authors took responsibility for data analysis, interpretation, and discussion of results. The authors read and approved the final manuscript.

**Funding** – No funding information from the authors.

**Availability of data and materials** - All data is available from the authors.

**Competing interests** - The authors declare no competing interests.

**Additional information** – No additional information from the authors.

## References

- [1] M. Vishnukumar, V. Muthupandi, and S. Jerome, "Microstructural characteristics, mechanical properties and corrosion performance of super austenitic stainless steel 904L produced by wire arc additive manufacturing," *Materials Today Communications*, vol. 35, p. 105801, Jun. 2023, doi: 10.1016/j.mtcomm.2023.105801.
- [2] Y. D. B. A. Puraditya, D. D. Mahendra, and P. H. Setyarini, "Characteristics of Bio-ceramic Coating on Corrosion Rate of Stainless Steel 316L and Titanium (Ti-6Al-4V)," *Mechanics Exploration and Material Innovation*, vol. 1, no. 1, pp. 20–26, Jan. 2024, doi: 10.21776/ub.memi.2024.001.01.3.
- [3] Y. Hu et al., "Crevice Corrosion Behavior of Stainless Steels in a Flue Gas Desulfurization Environment," *Journal of Materials Engineering and Performance*, vol. 32, no. 23, pp. 10567–10581, Dec. 2023, doi: 10.1007/s11665-023-07888-4.
- [4] K. Chandra, A. P. Singh, A. Mahanti, N. Kumar, V. Gautam, and V. Kain, "Comparative corrosion behaviour of stainless steels and their welds in wet-process phosphoric acid," *Corrosion Engineering, Science and Technology*, vol. 56, no. 5, pp. 483–494, Jul. 2021, doi: 10.1080/1478422X.2021.1916237.
- [5] N. P. Parahdiba, H. Salafy, A. Marizki, and A. N. Camila, "Effect of Heat Treatment Variation on Grain Boundary Corrosion of Austenitic Stainless Steel," *Mechanics Exploration and Material Innovation*, vol. 1, no. 3, pp. 94–101, 2024, doi: 10.21776/ub.memi.2024.001.03.4.
- [6] C. Wang et al., "Crevice Corrosion Behavior of Several Super Stainless Steels in a Simulated Corrosive Environment of Flue Gas Desulfurization Process," *Journal of Chinese Society for Corrosion and Protection*, vol. 39, no. 1, pp. 43–50, 2019, doi: 10.11902/1005.4537.2017.215.
- [7] A. Rajesh Kannan, S. Mohan Kumar, N. Pravin Kumar, N. Siva Shanmugam, A. S. Vishnu, and Y. Palguna, "Process-microstructural features for tailoring fatigue strength of wire arc additive manufactured functionally graded material of SS904L and Hastelloy C-276," *Materials Letters*, vol. 274, p. 127968, Sep. 2020, doi: 10.1016/j.matlet.2020.127968.

- [8] R. van der Merwe, "Corrosion characteristics of mild steel storage tanks in fluorine-containing acid," *Journal of the Southern African Institute of Mining and Metallurgy*, vol. 116, no. 10, pp. 921–926, 2016, doi: 10.17159/2411-9717/2016/v116n10a5.
- [9] N. Rojas et al., "Coated stainless steels evaluation for bipolar plates in PEM water electrolysis conditions," *International Journal of Hydrogen Energy*, vol. 46, no. 51, pp. 25929–25943, Jul. 2021, doi: 10.1016/j.ijhydene.2021.03.100.
- [10] K. Venkatesan et al., "Investigation of machining performance in SS904L alloy under hybrid cooling conditions," *Canadian Metallurgical Quarterly*, pp. 1–19, Oct. 2024, doi: 10.1080/00084433.2024.2413242.
- [11] S. Rajendran, A. R. Kannan, B. Suresha, and N. S. Shanmugam, "Studies on the Fatigue Performance of Wire and Arc Additive Manufactured SS 904L," in *Proceedings of the International Conference on Industrial and Manufacturing Systems (CIMS-2020)*, 2022, pp. 343–352. doi: 10.1007/978-3-030-73495-4\_24.
- [12] A. Rajesh Kannan, S. Mohan Kumar, R. Pramod, N. Pravin Kumar, N. Siva Shanmugam, and Y. Palguna, "Microstructure and mechanical properties of wire arc additive manufactured bi-metallic structure," *Science and Technology of Welding and Joining*, vol. 26, no. 1, pp. 47–57, Jan. 2021, doi: 10.1080/13621718.2020.1833140.
- [13] M. Forouzanmehr et al., "Detection and Analysis of Corrosion and Contact Resistance Faults of TiN and CrN Coatings on 410 Stainless Steel as Bipolar Plates in PEM Fuel Cells," *Sensors*, vol. 22, no. 3, p. 750, Jan. 2022, doi: 10.3390/s22030750.
- [14] S. S. Prabu, K. D. Ramkumar, and N. Arivazhagan, "Investigation on the fusion zone microstructures and mechanical integrity of AISI 904L and Inconel 625 weld joints," *Materials Research Express*, vol. 6, no. 8, p. 086540, May 2019, doi: 10.1088/2053-1591/ab1883.
- [15] H. Dai, S. Shi, L. Yang, C. Guo, and X. Chen, "Recent progress on the corrosion behavior of metallic materials in HF solution," *Corrosion Reviews*, vol. 39, no. 4, pp. 313–337, Aug. 2021, doi: 10.1515/corrrev-2020-0101.
- [16] T. Zhao et al., "Cavitation erosion/corrosion synergy and wear behaviors of nickel-based alloy coatings on 304 stainless steel prepared by cold metal transfer," *Wear*, vol. 510–511, p. 204510, Dec. 2022, doi: 10.1016/j.wear.2022.204510.
- [17] L. D. Bobbio, B. Bocklund, Z.-K. Liu, and A. M. Beese, "Tensile behavior of stainless steel 304L to Ni-20Cr functionally graded material: Experimental characterization and computational simulations," *Materialia*, vol. 18, p. 101151, Aug. 2021, doi: 10.1016/j.mtla.2021.101151.
- [18] Y. Leng, D. Yang, P. Ming, and C. Zhang, "A comparative study of corrosion resistance evaluation of bipolar plate materials for proton exchange membrane fuel cell," *eTransportation*, vol. 10, p. 100139, Nov. 2021, doi: 10.1016/j.etrans.2021.100139.
- [19] S. Mohan Kumar et al., "Microstructural Features and Mechanical Integrity of Wire Arc Additive Manufactured SS321/Inconel 625 Functionally Gradient Material," *Journal of Materials Engineering and Performance*, vol. 30, no. 8, pp. 5692–5703, Aug. 2021, doi: 10.1007/s11665-021-05617-3.
- [20] T. S. Senthil, S. Ramesh Babu, M. Puviyarasan, and V. Dhinakaran, "Mechanical and microstructural characterization of functionally graded Inconel 825 - SS316L fabricated using wire arc additive manufacturing," *Journal of Materials Research and Technology*, vol. 15, pp. 661–669, Nov. 2021, doi: 10.1016/j.jmrt.2021.08.060.
- [21] R. Aslam, M. Mobin, S. Zehra, and J. Aslam, "A comprehensive review of corrosion inhibitors employed to mitigate stainless steel corrosion in different environments," *Journal of Molecular Liquids*, vol. 364, p. 119992, Oct. 2022, doi: 10.1016/j.molliq.2022.119992.
- [22] O. Sanni, A. P. I. Popoola, and O. S. I. Fayomi, "The inhibitive study of egg shell powder on uns n08904 austenitic stainless steel corrosion in chloride solution," *Defence Technology*, vol. 14, no. 5, pp. 463–468, Oct. 2018, doi: 10.1016/j.dt.2018.07.015.